Supplementary Information (SI) for Dalton Transactions.

Supporting Information

Strong second-harmonic generation response in an organic-inorganic hybrid antimony bromide

Xuemei Wen,[†] Gangji Yi,[†] Qinglan Zhong,[†] Caihong Guo,*[,†] Guohong Zou,[†] Hongmei Zeng,[†] and Zhien Lin*[,†]

[†] College of Chemistry, Sichuan University, Chengdu 610064, China

* To whom correspondence should be addressed. Tel: +86-28-85412284. E-mail: guocaihong@scu.edu.cn, zhienlin@scu.edu.cn

Synthesis

Antimony(III) chloride ($SbCl_3$, 99%, MACKLIN), nicotinic acid ($C_6H_5NO_2$, 99%, MACKLIN), hydrobromic acid (HBr, 48%, MACKLIN), methanol (CH_3OH, AR, CHRON) were commercially available and used without further purification.

$(C_6H_6NO_2)_2Sb_2Br_8\cdot H_2O$ (**1**) and $(C_6H_6NO_2)_2SbBr_5$ (**2**) were synthesized as follows: the single crystals of compounds **1** and **2** were harvested by a facile solvent evaporation method. For compound **1**, $SbCl_3$ (0.114 g, 0.5 mmol), nicotinic acid (0.062 g, 0.5 mmol), HBr (228 μL, 2 mmol), and methanol (1.5 mL) were mixed in a 10 mL glass beaker. After slow evaporation at 45 °C for two days, block crystals were obtained with a 45% yield based on antimony. Similarly, when the amount of HBr was increased to 285 μL (2.5 mmol) while keeping other conditions the same, plate crystals of compound **2** were obtained with a 65% yield based on antimony.

Structural determination

Single crystal X-ray diffraction data were collected on Bruker D8 Venture diffractometer at room temperature. The crystal structures were solved by direct methods. The structures were refined on F^2 by full-matrix least-squares methods using the *SHELXTL* program package.[1, 2]

Powder XRD analysis

Powder X-ray diffraction data were obtained using a Shimazu XRD-6100 diffractometer with Cu-Kα radiation ($\lambda = 1.5418$ Å), in the angular range of $2\theta = 5-50°$, and with a scan step width of 0.02° and a fixed time of 0.2 s.

Thermal Stability Analysis

Thermal analysis was performed in a dynamic nitrogen atmosphere using a Shimadzu DTG-60H thermal analyzer with a heating rate of 10 ºC/min in the range of 30 to 800 ºC.

IR Spectroscopy

IR spectra of compounds **1** and **2** were obtained on a Nicolet Impact 4100 FTIR spectrometer by using KBr pellets, with transmission mode from 4000 to 400 cm^{-1}.

UV-Vis Diffuse Reflectance Spectroscopy

The UV−vis diffuse reflectance spectra of title compounds were recorded at room temperature on a Shimadzu UV-2600 UV−vis spectrophotometer in the wavelength range of 200–800 nm. $BaSO_4$ powder was used as 100% reflectance reference. The Kubelka-Munk function[3, 4] was used to calculate the absorption spectra from the reflection spectra: $F(R) = \alpha/S = (1\text{-}R)^2/2R$, where R is the reflectance, α is the absorption coefficient, and S is the scattering coefficient.

Birefringence Measurements

The birefringences of compounds **1** and **2** were characterized by using the polarizing microscope equipped (ZEISS Axio Scope. A1) with a Berek compensator.

Second-Harmonic Generation Tests

The Kurtz and Perry method was used to measure powder second harmonic generation (SHG) signals at room temperature.[5] The SHG efficiency mainly depends on the particle size, and the crystalline compound was ground and divided into the following particle sizes: 25–45, 45–58, 58–75, 75–106, 106–150 and 150–212 μm. Microcrystalline KH_2PO_4 (KDP) with the same particle size was used as a reference. The measurements were performed using Q-switched Nd: YAG lasers with visible light at 1064 nm, and a cut-off filter was used to limit the background flash light on the sample, and the SHG signal is recorded by a photomultiplier tube.

Computational Methods

In order to understand the relationship between structure and properties of compounds **1**,

2, the first-principles calculations were carried out by using the CASTEP software package.[6] The band structure, density of states (DOS) / partial density of states (PDOS), and optical properties of compounds **1** and **2** were calculated. The generalized gradient approximation (GGA) with Perdew-Burke-Ernzer (PBE) was used for all the calculations.[7] All the atoms were performed by Norm-conserving pseudopotentials (NCP), with H $1s^1$, C $2s^22p^2$, N $2s^22p^3$, O $2s^22p^4$, Br $4s^24p^5$, Sb $5s^25p^3$ treated as valence electrons.[8] The kinetic energy cutoff of 750 eV and the k-point sampling of 4 × 4 × 3 were chosen for the compound **1**. The k-point sampling of 2 × 2 × 4 were chosen for the compound **2**.[9] All other parameter settings are CASTEP default values.

To obtain the linear optical properties, the complex dielectric function $\varepsilon(\omega) = \varepsilon_1(\omega) + i\varepsilon_2(\omega)$ has been determined in the random phase approximation from the PBE wavefunctions. The imaginary part of the dielectric function due to direct inter-band transitions is given by the expression,

$$\varepsilon_2(\hbar\omega)=\frac{2e^2\pi}{\Omega\varepsilon_0}\sum_{k,v,c}\left|\langle\psi_k^c|u\cdot r|\psi_k^v\rangle\right|^2\delta(E_k^c-E_k^v-E)$$

(equation S1)

where Ω, ω, u, v and c are the unit-cell volume, photon frequencies, the vector defining the polarization of the incident electric field, valence and conduction bands, respectively. The real part of the dielectric function is obtained from ε_2 by a Kramers-Kronig transformation,

$$\varepsilon_1(\omega)=1+(\frac{2}{\pi})\int_0^{+\infty}d\omega'\frac{\omega'^2\varepsilon_2(\omega)}{\omega'^2-\omega^2}$$

(equation S2)

In calculation of the static $\chi^{(2)}$ coefficients, the so-called length-gauge formalism derived by Aversa and Sipe [10] and modified by Rashkeev *et al* [11] is adopted, which has been proved to be successful in calculating the second order susceptibility for semiconductors and insulators.[12, 13] In the static case, the imaginary part of the static second-order optical susceptibility can be expressed as:

$$\chi^{abc} = \frac{e^3}{\hbar^2\Omega}\sum_{nml,k}\frac{r^a_{nm}(r^b_{ml}r^c_{ln}+r^c_{ml}r^b_{ln})}{2\omega_{nm}\omega_{ml}\omega_{ln}}[\omega_n f_{ml}+\omega_m f_{ln}+\omega_l f_{nm}] + \frac{ie^3}{4\hbar^2\Omega}\sum_{nm,k}\frac{f_{nm}}{\omega^2_{mn}}[r^a_{nm}(r^b_{mn;c}+r^c_{mn;b})+r^b_{nm}(r^a_{mn;c}+r^c_{mn;a})+r^c_{nm}(r^a_{mn;b}+r^b_{mn;a})]$$

(equation S3)

where r is the position operator, $\hbar\omega_{nm} = \hbar\omega_n - \hbar\omega_m$ is the energy difference for the bands m and n, $f_{mn} = f_m - f_n$ is the difference of the Fermi distribution functions, subscripts a, b, and c are Cartesian indices, and $r^b_{mn;a}$ is the so-called generalized derivative of the coordinate operator in k space,

$$r^b_{nm;a} = \frac{r^a_{nm}\Delta^b_{mn}+r^b_{nm}\Delta^a_{mn}}{\omega_{nm}} + \frac{i}{\omega_{nm}}\times\sum_l(\omega_{lm}r^a_{nl}r^b_{lm} - \omega_{nl}r^b_{nl}r^a_{lm})$$

(equation S4)

where $\Delta^a_{nm} = (p^a_{nn} - p^a_{mm}) / m$ is the difference between the electronic velocities at the bands n and m.

Table S1. Bond lengths [Å] for compounds **1** and **2**.

compound **1**		compound **2**	
Sb1-Br1	2.6196(11)	Sb1-Br1	3.1200(19)
Sb1-Br2	2.5658(12)	Sb1-Br2	2.6181(18)
Sb1-Br3	2.5516(10)	Sb1-Br3	2.6161(18)
Sb1-Br4	3.0212(12)	Sb1-Br4	2.6685(19)
Sb1-Br5	3.1800(11)	Sb1-Br5	2.923(2)
Sb2-Br4	3.0158(14)	O1-C1	1.244(19)
Sb2-Br5	3.1091(10)	O2-C1	1.26(2)
Sb2-Br6	2.6161(12)	O3-C7	1.233(18)
Sb2-Br7	2.5870(11)	O4-C7	1.25(2)
Sb2-Br8	2.5189(11)	N1-C5	1.3900
O1-C1	1.210(10)	N1-C6	1.3900
O2-C1	1.304(11)	N2-C11	1.3900
O3-C7	1.233(10)	N2-C12	1.3900
O4-C7	1.274(10)	C1-C2	1.446(19)
N1-C5	1.316(14)	C2-C3	1.3900
N1-C6	1.352(13)	C2-C6	1.3900
N2-C11	1.334(11)	C3-C4	1.3900
N2-C12	1.297(10)	C4-C5	1.3900
C1-C2	1.488(13)	C7-C8	1.478(19)
C2-C3	1.375(13)	C8-C9	1.3900
C2-C6	1.385(12)	C8-C12	1.3900
C3-C4	1.385(13)	C9-C10	1.3900
C4-C5	1.378(14)	C10-C11	1.3900
C7-C8	1.502(11)		
C8-C9	1.369(11)		
C8-C12	1.375(11)		
C9-C10	1.392(13)		
C10-C11	1.363(13)		

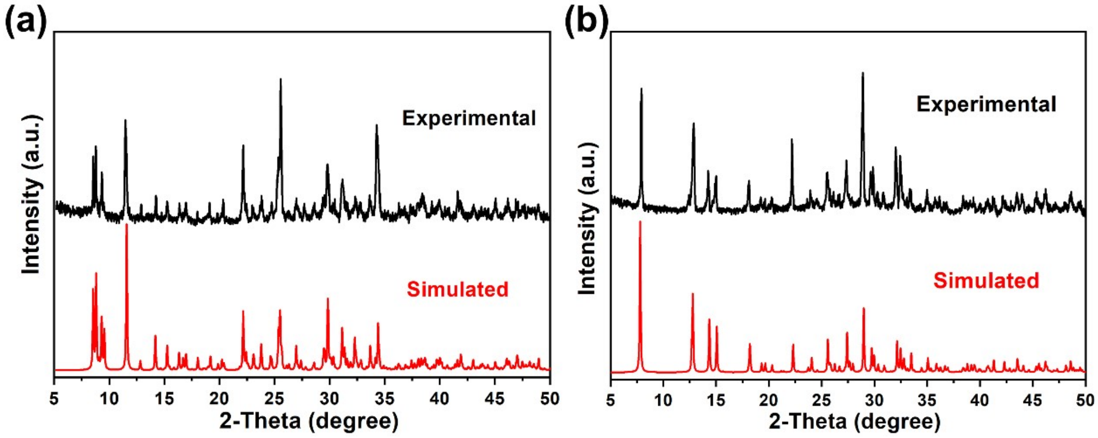

Fig. S1 Simulated and experimental powder XRD patterns for compounds **1** (a) and **2** (b).

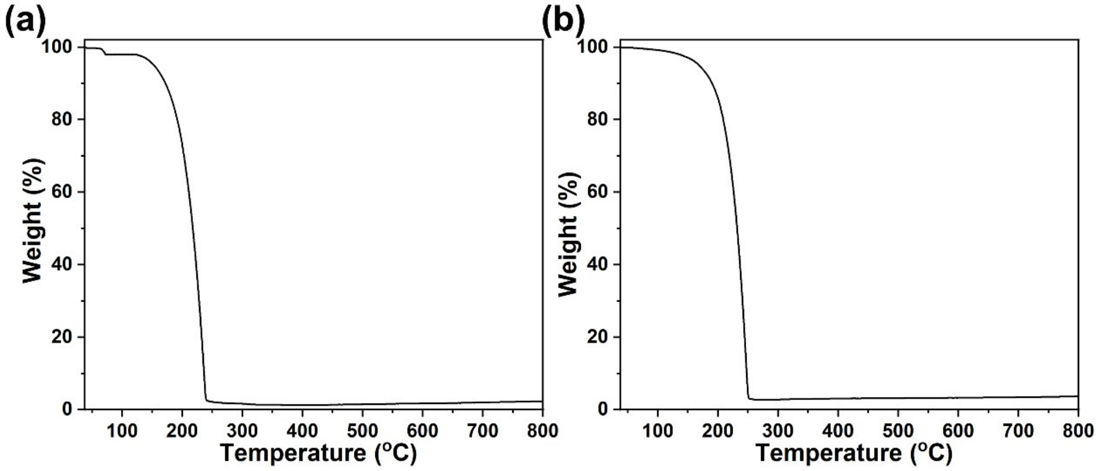

Fig. S2 TGA curves of compounds **1** (a) and **2** (b).

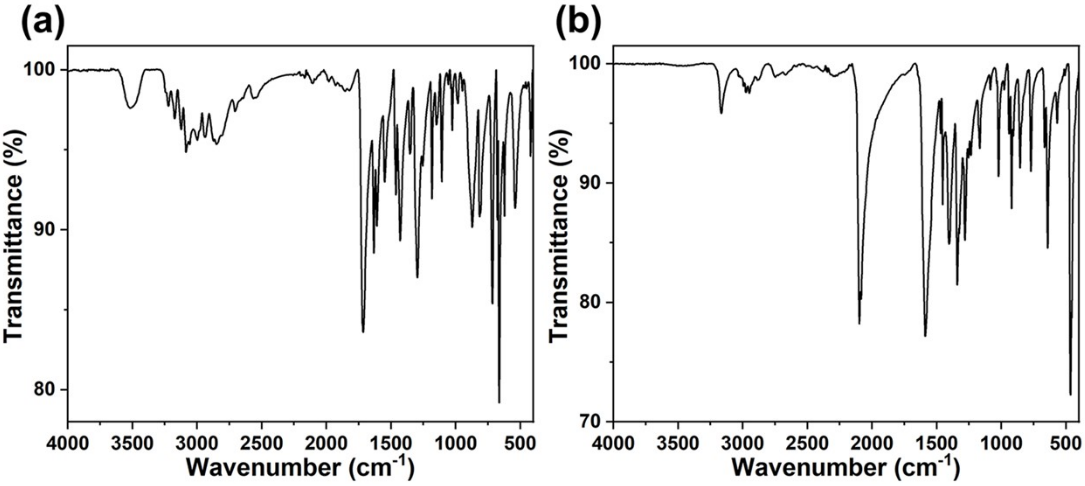

Fig. S3 IR spectra of compounds **1** (a) and **2** (b).

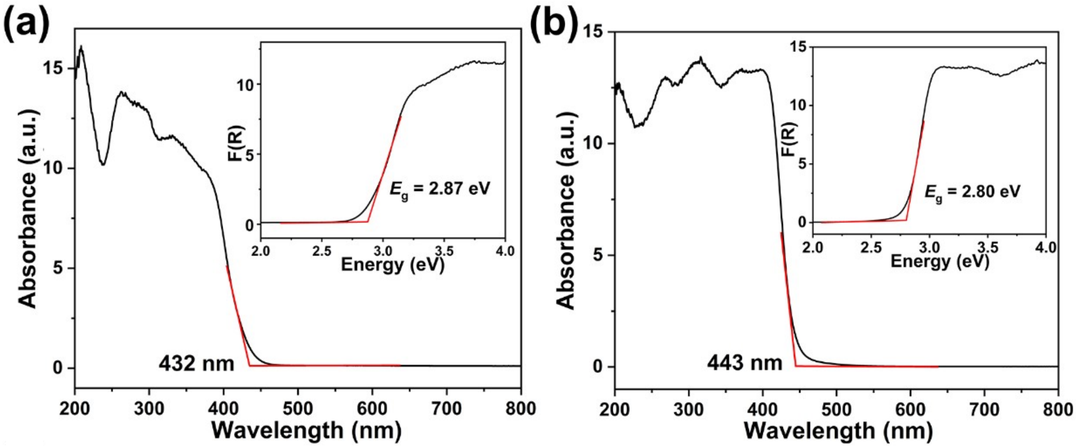

Fig. S4 UV-vis absorption spectra for compounds **1** (a) and **2** (b).

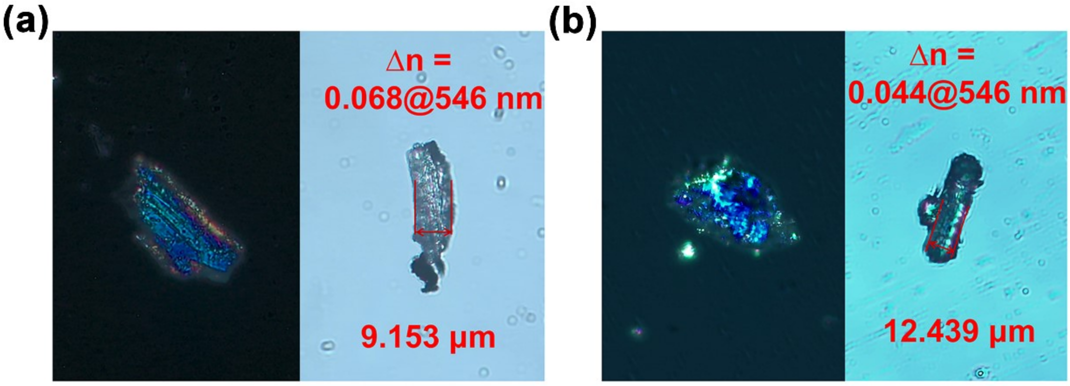

Fig. S5 Birefringence measurements for compounds **1** (a) and **2** (b) performed using a polarizing microscope.

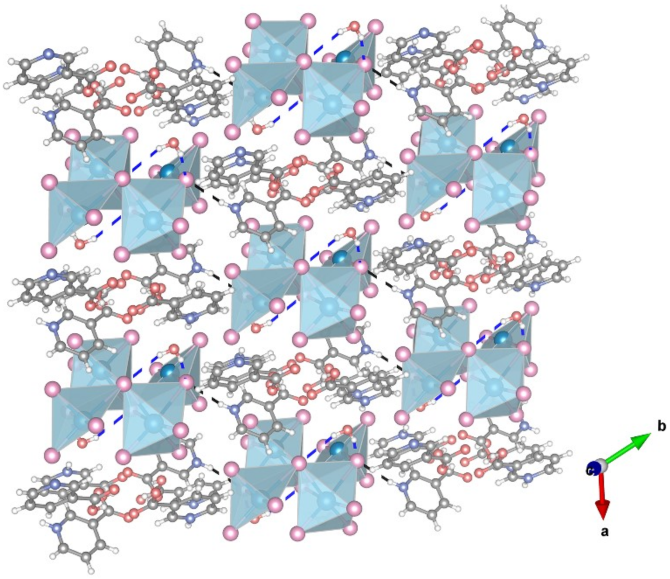

Fig. S6 A supramolecular three-dimensional structure formed by hydrogen bond interactions in compound **1** (black dashed lines: N–H···Br hydrogen bonds, blue dashed lines: O–H···Br hydrogen bonds).

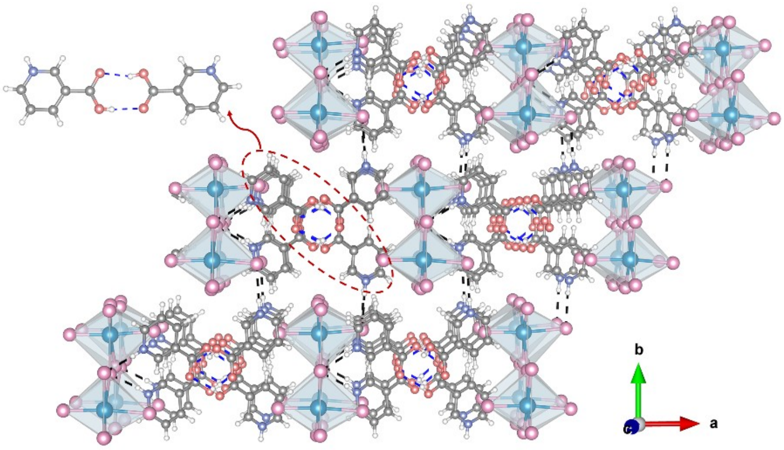

Fig. S7 A supramolecular three-dimensional structure formed by hydrogen bond interactions in compound **2** (black dashed lines: N–H···Br hydrogen bonds, blue dashed lines: O–H···O=C hydrogen bonds).

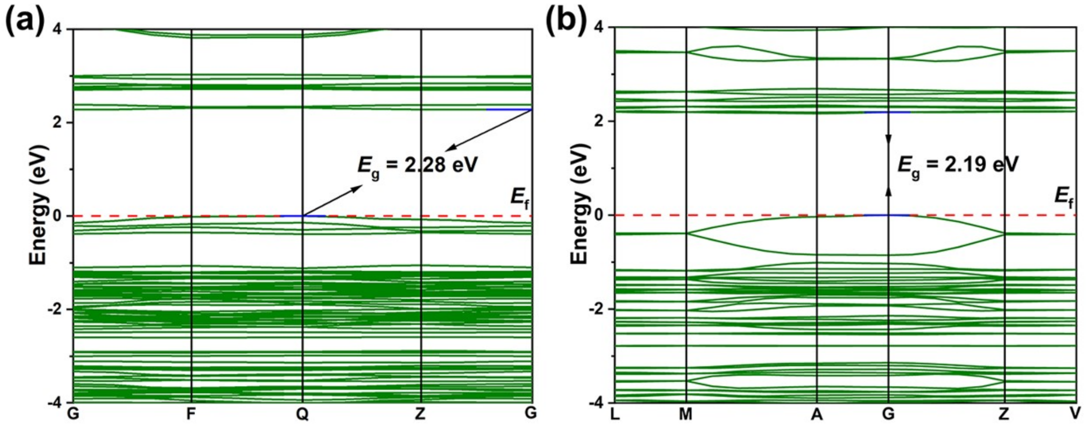

Fig. S8 Calculated band structures for compounds **1** (a) and **2** (b) (the Ferm level is set at 0 eV).

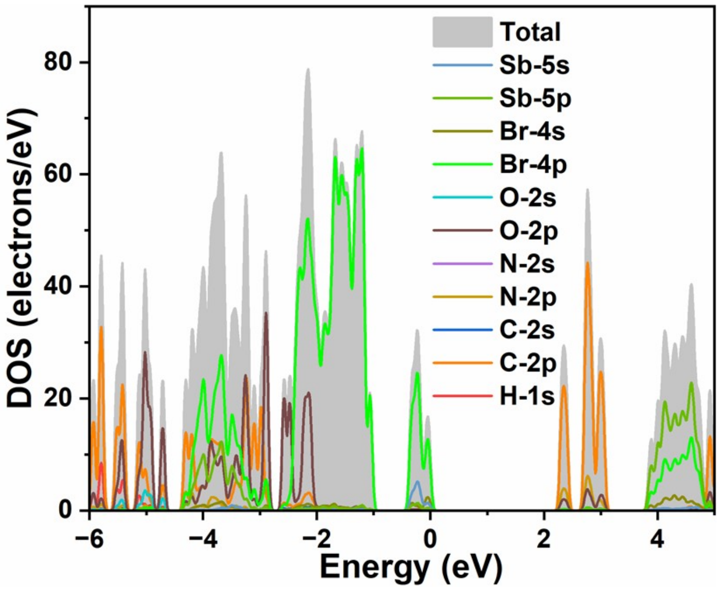

Fig. S9 Total and partial DOS of compound **1**.

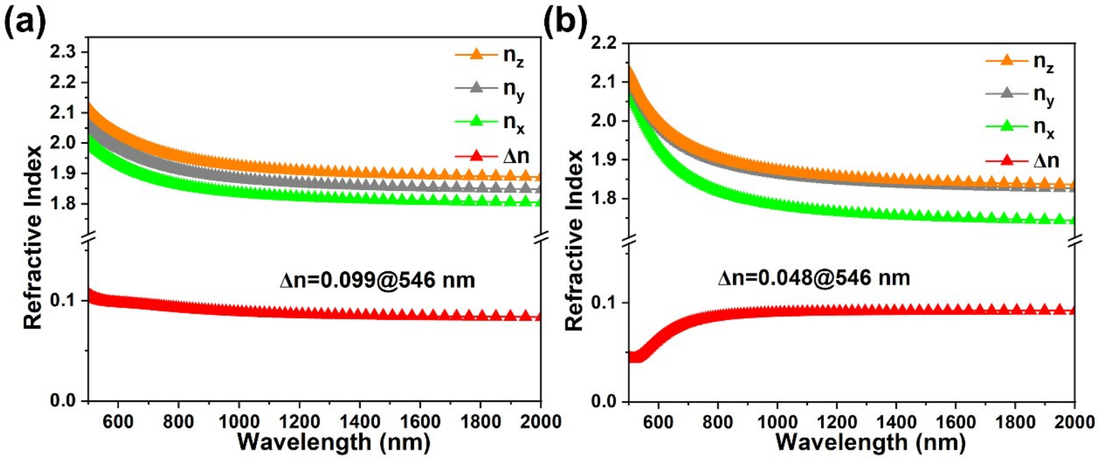

Fig. S10 The calculated linear refractive indices of compounds **1** (a) and **2** (b).

References

(1) G. M. Sheldrick, *Acta Crystallogr. Sect. A,* 2015, **71**, 3.

(2) G. M. Sheldrick, *Acta Crystallogr. Sect. A,* 2008, **64**, 112.

(3) P. Kubelka and F. Munk, *Z. Technol. Phys.,* 1931, **12**, 593.

(4) J. Tauc, *Mater. Res. Bull.,* 1970, **5**, 721.

(5) S. K. Kurtz and T. T. Perry, *J. Appl. Phys.,* 1968, **39**, 3798.

(6) M. D. Segall, P. J. D. Lindan, M. J. Probert, C. J. Pickard, P. J. Hasnip, S. J. Clark and M. C. Payne, *J. Phys. Condens. Matter,* 2002, **14**, 2717.

(7) J. P. Perdew, K. Burke and M. Ernzerhof, *Phys. Rev. Lett.,* 1996, **77**, 3865.

(8) K. Kobayashi, *Comput. Mater. Sci.,* 1999, **14**, 72.

(9) D. Vanderbilt, *Phys. Rev. B,* 1990, **41**, 7892.

(10) G. Kresse, VASP, 5.3.5; http://cms.mpi.univie.ac.at/vasp/vasp/vasp.html. 2014.

(11) S. N. Rashkeev, W. R. L. Lambrecht and B. Segall, *Phys. Rev. B,* 1998, **57**, 3905.

(12) B. Champagne and D. M. Bishop, *Adv. Chem. Phys.,* 2003, **126***,* 41.

(13) A. H. Reshak, S. Auluck and I. V. Kityk, *Phys. Rev. B: Condens. Matter Mater. Phys.,* 2007, **75**, 245120.